Electronic Supplementary Material (ESI) for Dalton Transactions.
This journal is © The Royal Society of Chemistry 2017

Novel half-sandwich iridium(III) imino-pyridyl complexes showing remarkable in vitro anticancer activity

JuanJuan Li, Lihua Guo, Zhenzhen Tian, Meng Tian, Shumiao Zhang, Ke Xu, Yuchuan Qian, Zhe Liu*

Institute of Anticancer Agents Development and Theranostic Application, The Key Laboratory of Life-Organic Analysis and Key Laboratory of Pharmaceutical Intermediates and Analysis of Natural Medicine, Department of Chemistry and Chemical Engineering, Qufu Normal University, Qufu 273165, China.

*Corresponding author. Email: liuzheqd@163.com

Supporting Information

EXPERIMENTAL SCETION

Materials and Instrumentation. $IrCl_3 \cdot nH_2O$, 2,3,4,5-tetramethyl-2-cyclopentenone (95%), 1,2,3,4,5-pentamethyl-cyclopentadiene (95%), butyllithium solution (1.6 M in hexane), 2,6-dimethylaniline, 2,6-diisopropylaniline, 1-(pyridin-2-yl)ethanone, picolinaldehyde, quinoline-2-carbaldehyde, 9-ethylguanine, and 9-methyladenine were purchased from Sigma-Aldrich. Dimers 1-2[16] and ligand L_2[55] were prepared as described. For the biological experiments, BSA, CT-DNA, pBR322 plasmid DNA, DMEM medium, fetal bovine serum, penicillin/streptomycin mixture, trypsin/EDTA, and phosphate-buffered saline (PBS) were purchased from Sangon Biotech. Testing compounds was dissolved in DMSO and diluted with the tissue culture medium before use.

X-ray Crystallography. All diffraction data were obtained on a Bruker Smart Apex CCD diffractometer equipped with graphite-monochromated Mo Kα radiation. Absorption corrections were applied using SADABS program. The crystals were mounted in oil and held at 100 K with the Oxford Cryosystem Cobra. The structures were solved by direct methods using SHELXS (TREF) with additional light atoms found by Fourier methods. Complexes were refined against F2using SHELXL, and hydrogen atoms were added at calculated positions and refined riding on their parent atoms. X-ray crystallographic data for complexes **2A**, **2B** and **3A** are available as **Figure 1**, **Tables 1-2** and have been deposited in the Cambridge Crystallographic Data Centre under the accession numbers 1558347 (**2A**),1558348 (**2B**), 1558349 (**3A**). X-ray crystallographic data in CIF format are available from the Cambridge Crystallographic Data Centre.

NMR Spectroscopy. ^{1}H NMR spectra were acquired in 5 mm NMR tubes at 310 K on Bruker DPX 500 (^{1}H = 500.13 MHz) spectrometers. ^{1}H NMR chemical shifts were internally referenced to $(CHD_2)(CD_3)SO$ (2.50 ppm) for DMSO-d_6, $CHCl_3$ (7.26 ppm) for chloroform-d_1. All data processing was carried out using XWIN-NMR version 3.6 (Bruker UK Ltd.).

UV-vis Spectroscopy. A TU-1901 UV-vis recording spectrophotometer was used with 1 cm path-length quartz cuvettes (3ml). Spectra were processed using UVWinlab software. Experiments were carried out at 298 K unless otherwise stated.

Hydrolysis Studies. Solutions of complexes **1A**-**4B** with final concentrations of 1 mM in 10% DMSO-d_6/90% D_2O (v/v) were prepared by dissolution of the complex in DMSO-d_6 followed by rapid dilution with D_2O. ^{1}H NMR spectra were recorded after various time intervals at 310 K. Solutions of complexes **1A**-**4B** with final concentrations of 50 μM in 5% MeOH/95% H_2O (v/v) were prepared by dissolution of the complex in MeOH followed by rapid dilution with H_2O. UV-Vis spectra of these solutions were recorded at 298 K after various time intervals.

Interactions with Nucleobases. The reaction of complexes **1A**-**4B** (ca. 1 mM) with nucleobases typically involved addition of a solution containing 1 mol equiv of nucleobase in D_2O to an equilibrium solution of complexes **1A**-**4B** in 20% MeOD /80% D_2O (v/v) . ^{1}H NMR spectra of these solutions were recorded at 310 K after various time intervals.

Cleavage of plasmid DNA. Gel electrophoresis experiments were carried out with pBR322 DNA, in 0.8% agarose solution, at 5 V/cm for 1.5 h using TAE buffer (40 mM Tris, 1 mM EDTA (Disodium Salt), pH 8.3). The pBR322 DNA was stained with 0.5 mg ml^{-1} gelred. The cleavage reactions were quenched by the addition of bromphenol blue. Gel electrophoresis was performed on a DYY-12C gel electrophoresis spectrometer. Agarose gel electrophoresis of pBR322 DNA was visualized using the gel imaging system (Smart Gel 600, China).

Interaction with ctDNA. Interaction of complexes with ctDNA was investigated by electronic

spectroscopy using spectrophotometric titration. Measurements were performed under physiological conditions (5 mM Tris–HCl/10 mM NaCl buffer solution, pH = 7.2) at ambient temperature with 5 min equilibration time. Spectra were collected from 200-700 nm after successive addition of ctDNA (0~0.3 mM) into 2 mL solution of complex (3.33 μM). ctDNA was compensated in the blank. Complexes were initially dissolved in dimethylsulfoxide (5 mM) and diluted with buffer to required concentration.

BSA binding experiments. The titration experiments including UV-Vis absorption and fluorescence quenching were performed at constant concentration of BSA. A BSA stock solution was prepared in Tris buffer (5 mM Tris–HCl/10 mM NaCl at pH 7.2) and stored at 4°C. All spectra were recorded after each successive addition of the compounds and incubation at room temperature for 5 min to complete the interaction. In the UV–Vis absorption titration experiment, a BSA solution (2.5 ml, 1×10^{-6} M) was titrated by successive additions of the stock solutions of Ir complex (1×10^{-3} M) and the changes in the BSA absorption were recorded after each addition. The fluorescence emission spectra of BSA in the absence and presence of Ir complex were also recorded with excitation at 285 nm. The concentrations of the Ir complex were 0–3.5 μM, and the concentration of BSA was fixed at 0.5 μM. Synchronous fluorescence spectra of BSA with various concentrations of complexes (0–50 μM) were obtained from 240 to 400 nm when $\Delta\lambda$ = 60 nm and from 255 to 400 nm when $\Delta\lambda$ = 15 nm.

Interaction with GSH. GSH (1.5 mol equiv) was added to an NMR tube containing a 2 mM solution of complex **2B** in 60% DMSO-d_6/40% D_2O at 310 K and N_2 atmosphere, ^{1}H NMR spectra of the resulting solutions were recorded at 310 K after various time intervals.

Reaction with NADH. When NADH (3.5 mol equiv) was added to a 1 mM solution of Ir complexes in 10% DMSO-d_6/90% D_2O (v/v), ^{1}H NMR spectra of these solutions were recorded at 298 K after various time intervals. The reaction of complexes (ca. 1 μM) with NADH (100 μM) in 10% MeOH/90% H_2O (v/v) was monitored by UV-Vis at 298 K after various time intervals. TON was calculated from the difference in NADH concentration after 7.5 h divided by the concentration of iridium catalyst. The concentration of NADH was obtained using the extinction coefficient ε_{339} = 6220 $M^{-1}cm^{-1}$.

Cell Culture. Hela human cervical cancer cells and A549 human lung cancer cells were obtained from Shanghai Institute of Biochemistry and Cell Biology (SIBCB) and were grown in Dubelco's Modified Eagle Medium (DMEM). All media were supplemented with 10% fetal bovine serum, and 1 % penicillin-streptomycin solution. All cells were grown at 310 K in a humidified incubator under a 5 % CO_2 atmosphere.

Viability assay (MTT assay). After plating 5000 A549 cells per well in 96-well plates, the cells were preincubated in drug-free media at 310 K for 24 h before adding different concentrations of the compounds to be tested. In order to prepare the stock solution of the drug, the solid complex was dissolved in DMSO. This stock was further diluted using cell culture medium until working concentrations were achieved. The drug exposure period was 24 h. Subsequently, 15 μl of 5 mg ml^{-1} MTT solution was added to form a purple formazan. Afterwards, 100 μl of dimethyl sulfoxide (DMSO) was transferred into each well to dissolve the purple formazan, and results were measured using a microplate reader (DNM-9606, Perlong Medical, Beijing, China) at an absorbance of 570 nm. Each well was triplicated and each experiment repeated at least three times. IC_{50} values quoted are mean ± SEM.

Cell Cycle Analysis. A549 cells at 1.5×10^6 per well were seeded in a six-well plate. Cells

were preincubated in drug-free media at 310 K for 24 h, after which drugs were added at concentrations of 0.25 × IC_{50} 0.5 × IC_{50} and 1 × IC_{50}. After 24 h of drug exposure, supernatants were removed by suction and cells were washed with PBS. Finally, cells were harvested using trypsin-EDTA and fixed for 24 h using cold 70 % ethanol. DNA staining was achieved by resuspending the cell pellets in PBS containing propidium iodide (PI) and RNAse. Cell pellets were washed and resuspended in PBS before being analyzed in a flow cytometer (ACEA NovoCyte, Hangzhou, China) using excitation of DNA-bound PI at 488 nm, with emission at 585 nm. Data were processed using NovoExpress™ software. The cell cycle distribution is shown as the percentage of cells containing G_0/G_1, S and G_2/M DNA as identified by propidium iodide staining.

Induction of Apoptosis. Flow cytometry analysis of apoptotic populations of A549 cells caused by exposure to iridium complexes was carried out using the Annexin V-FITC Apoptosis Detection Kit (Beyotime Institute of Biotechnology, China) according to the supplier's instructions. Briefly, A549 cells (1.5 ×10^6 /2 ml per well) were seeded in a six-well plate. Cells were preincubated in drug-free media at 310 K for 24 h, after which drugs were added at concentrations of 0.5 × $IC_{50,}$ 1 × $IC_{50,}$ 2 × IC_{50} and 3 × IC_{50}. After 24 h of drug exposure, cells were collected, washed once with PBS, and resuspended in 195 μl of annexin V-FITC binding buffer which was then added to 5 μl of annexin V-FITC and 10 μl of PI, and then incubated at room temperature in the dark for 15 min. Subsequently, the buffer placed in an ice bath in the dark. The samples were analyzed by a flow cytometer (ACEA NovoCyte, Hangzhou, China).

ROS Determination. Flow cytometry analysis of ROS generation in A549 cells caused by exposure to iridium complexes was carried out using the Reactive Oxygen Species Assay Kit (Beyotime Institute of Biotechnology, Shanghai, China) according to the supplier's instructions. Briefly, 1.5 × 10^6 A549 cells per well were seeded in a six-well plate. Cells were preincubated in drug-free media at 310 K for 24 h in a 5 % CO_2 humidified atmosphere, and then drugs were added at concentrations of 0.25 × IC_{50}. After 24 h of drug exposure, cells were washed twice with PBS and then incubated with the DCFH-DA probe (10 μM) at 37 °C for 30 min, and then washed triple immediately with PBS. The fluorescence intensity was analyzed by flow cytometry (ACEA NovoCyte, Hangzhou, China). Data were processed using NovoExpress™ software. At all times, samples were kept under dark conditions to avoid light-induced ROS production.

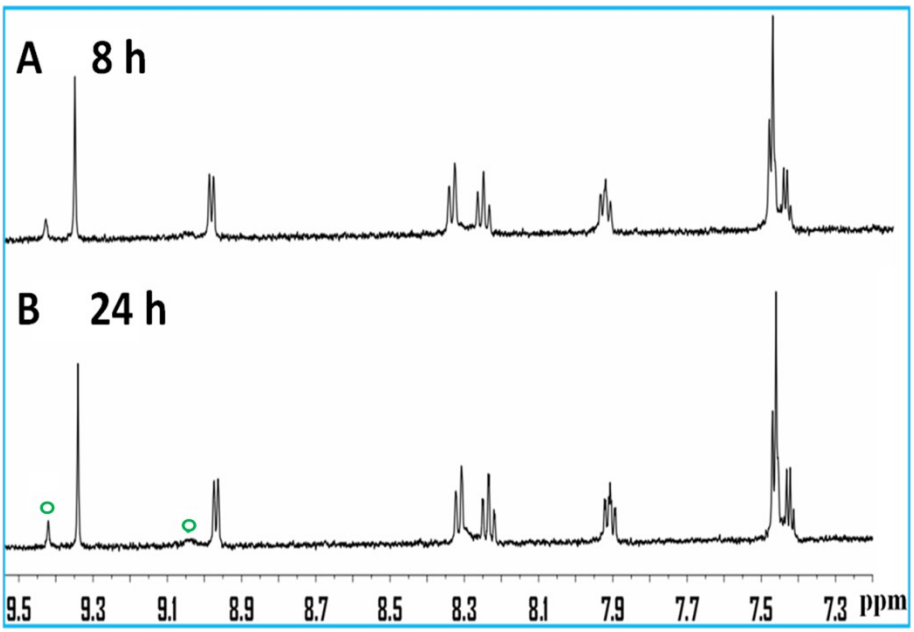

Figure S1. ^{1}H NMR spectra showing hydrolysis of complex [(η^5-C_5Me_5)Ir(L_2)Cl]PF_6 (**2A**) (1 mM) in 10% DMSO-d_6/90% D_2O (v/v) at 310 K after (A) 8 h; (B) 24 h. Peak assignments: green circles correspond to formed aqua complex after hydrolysis.

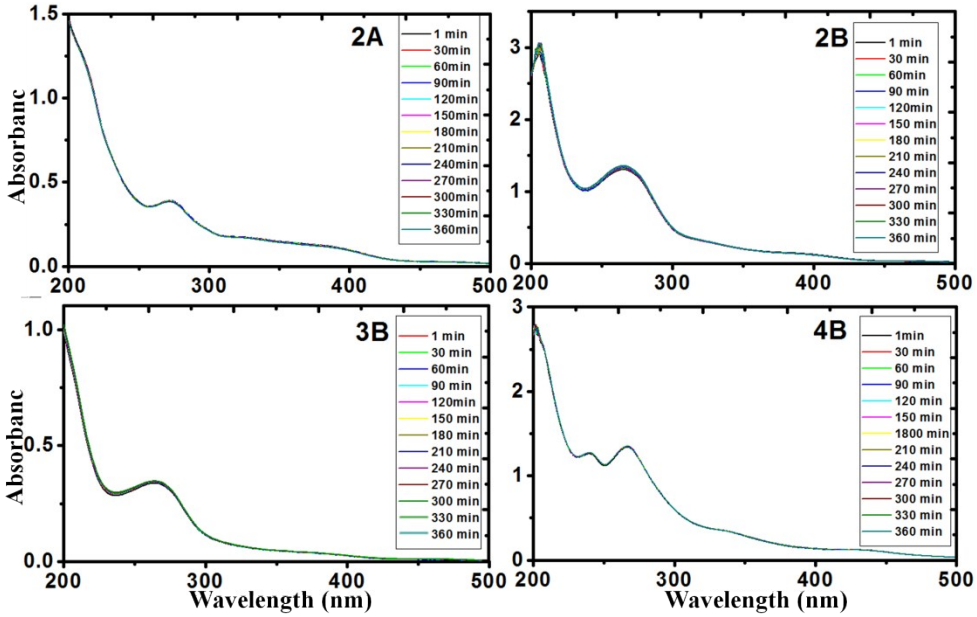

Figure S2. UV-Vis spectrum for a 50 μM solution of complexes **2A**, **2B**, **3B** and **4B** in 5% MeOH/95% H_2O (v/v) recorded over 6 h at 298 K.

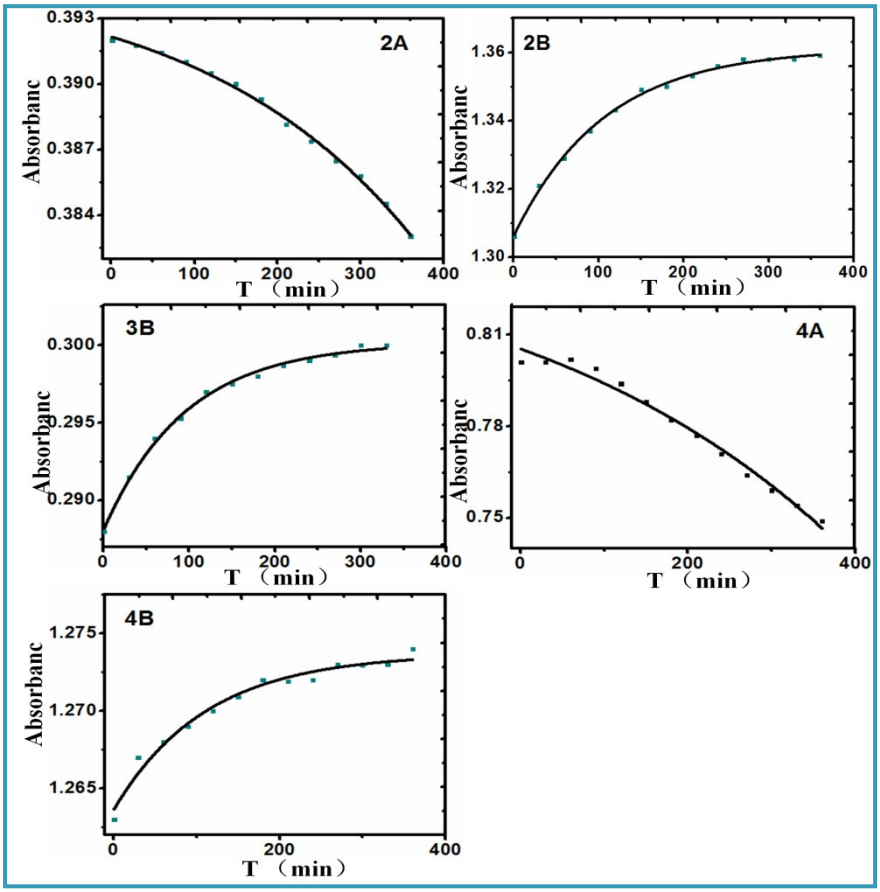

Figure S3. Time dependence of hydrolysis of **2A**, **2B**, **3B**, **4A** and **4B** in 5% MeOH/95% H_2O (v/v) at 298 K based on UV-Vis spectrum by measuring the absorption difference.

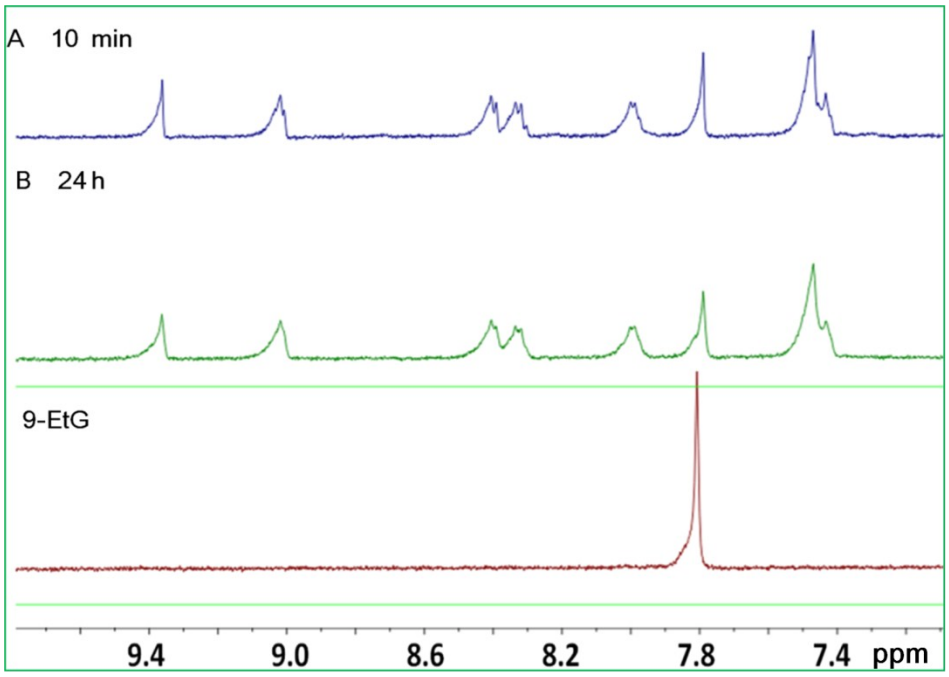

Figure S4. Low-field region of the^1 H NMR spectra for reaction of $[(\eta^5\text{-}C_5Me_5)Ir(L_3)Cl]PF_6$ **(3A)** with 9-EtG: (A) 10 min after addition of 1 mol equiv of 9-EtG to an equilibrium solution of complex **3A** (1.0 mM) in 20% MeOD-d_4 /80% D_2O (v/v) at 310 K; (B) after 24h.

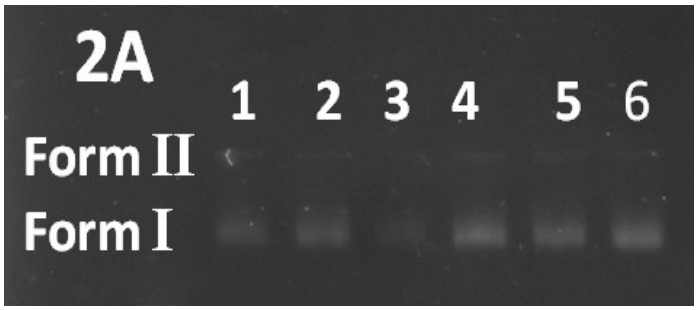

Figure S5. Agarose gel electrophoresis patterns for the cleavage of pBR322 DNA by various concentrations of complex **2A** at cleavage conditions: 10 μM DNA; 1 mM Tris–CH_3COOH buffer; pH 8; 37℃ for 24h. Lane 1: DNA control; Lane 2: DNA + 20 μM **2A**; Lane 3: DNA + 40 μM **2A**; Lane 4: DNA + 60 μM **2A**; Lane 5: DNA + 80 μM **2A**; Lane 6: DNA +100 μM **2A**.

A)

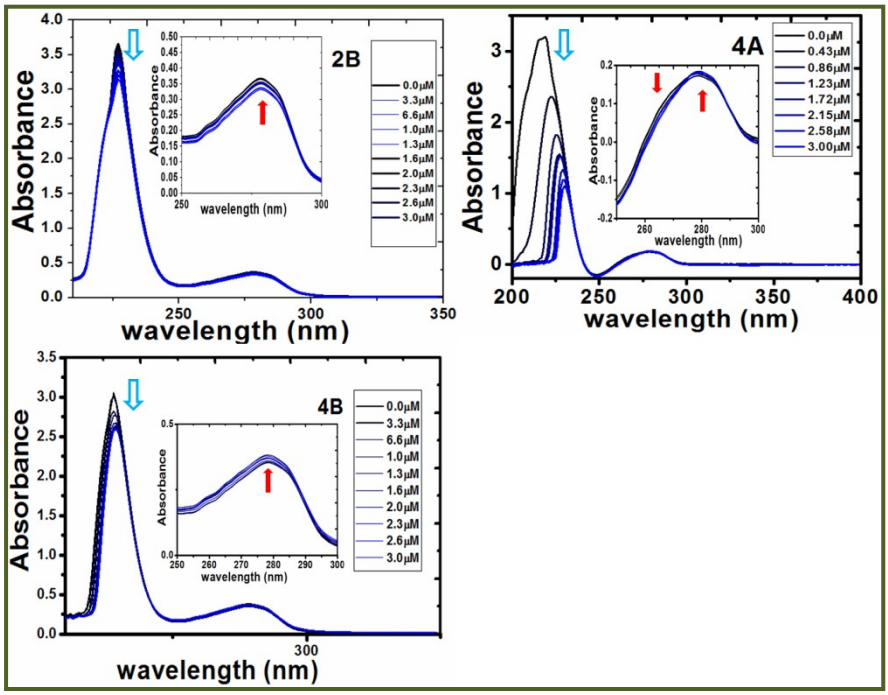

B)

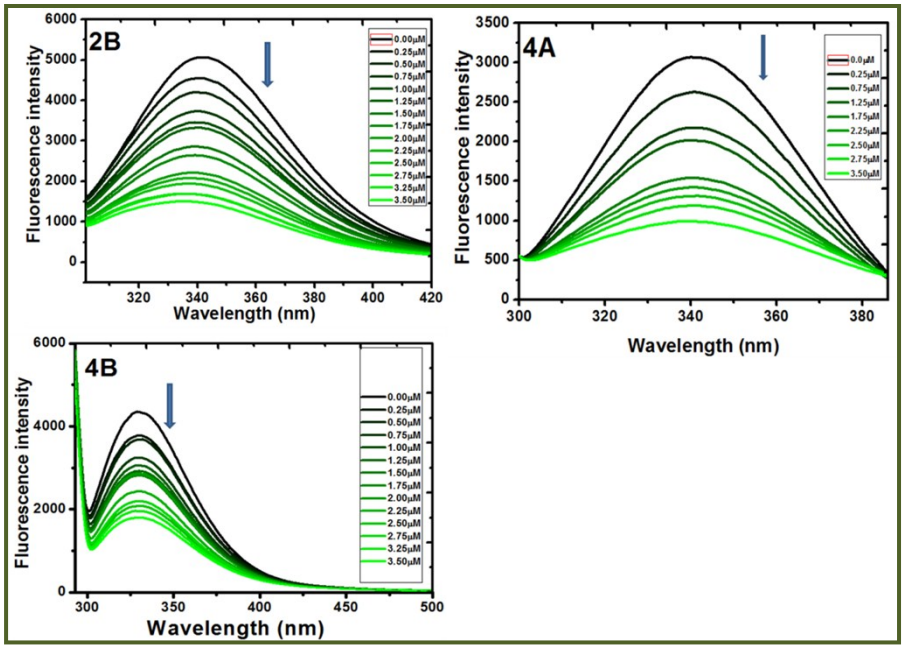

Figure S6. (A) Electronic absorption spectra of BSA in 5 mM Tris–HCl/10 mM NaCl buffer solution (pH = 7.2) upon addition of the Ir(III) complex (0–3.0 μM). The arrows show the direction of changes in absorbance upon increasing the concentration of the complex. (B) Fluorescence spectra of BSA in the absence and presence of the Ir(III) complex (0–3.5 μM). The arrow shows the intensity changes in increasing concentration of the Ir(III) complex.

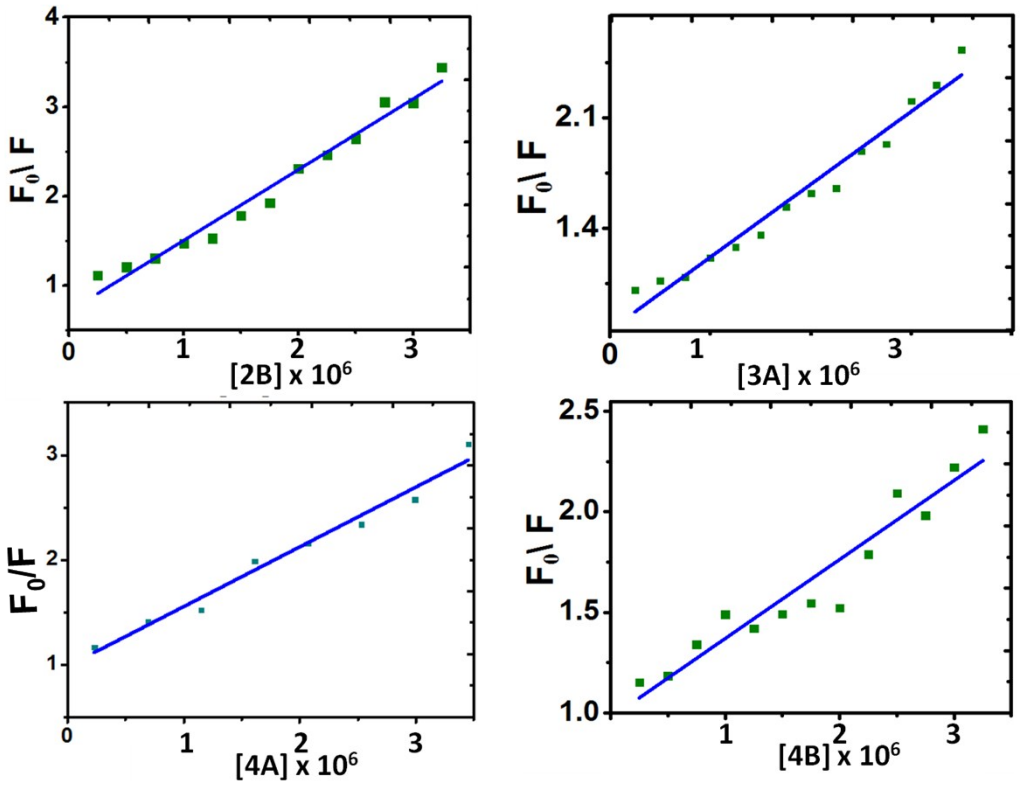

Figure S7. Stern–Volmer plots of F_0/F against the concentration of compounds **2B**, **3A**, **4A** and **4B**.

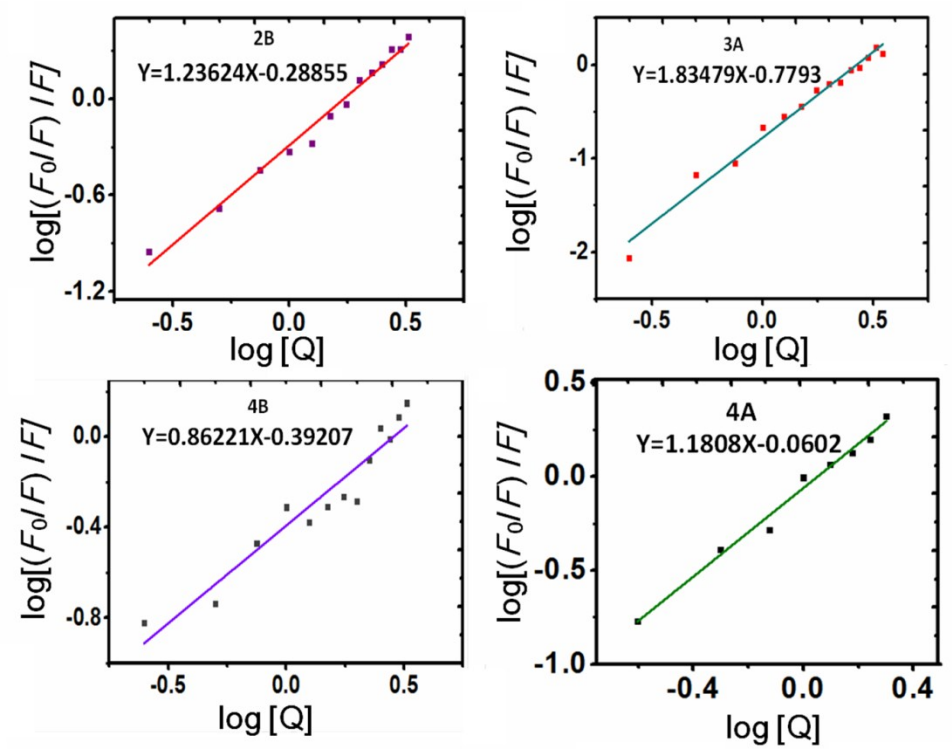

Figure S8. Plots of log[(F_0− F)/F] vs. log[Q] for the interaction of BSA with compounds **2B**, **3A**, **4A** and **4B**.

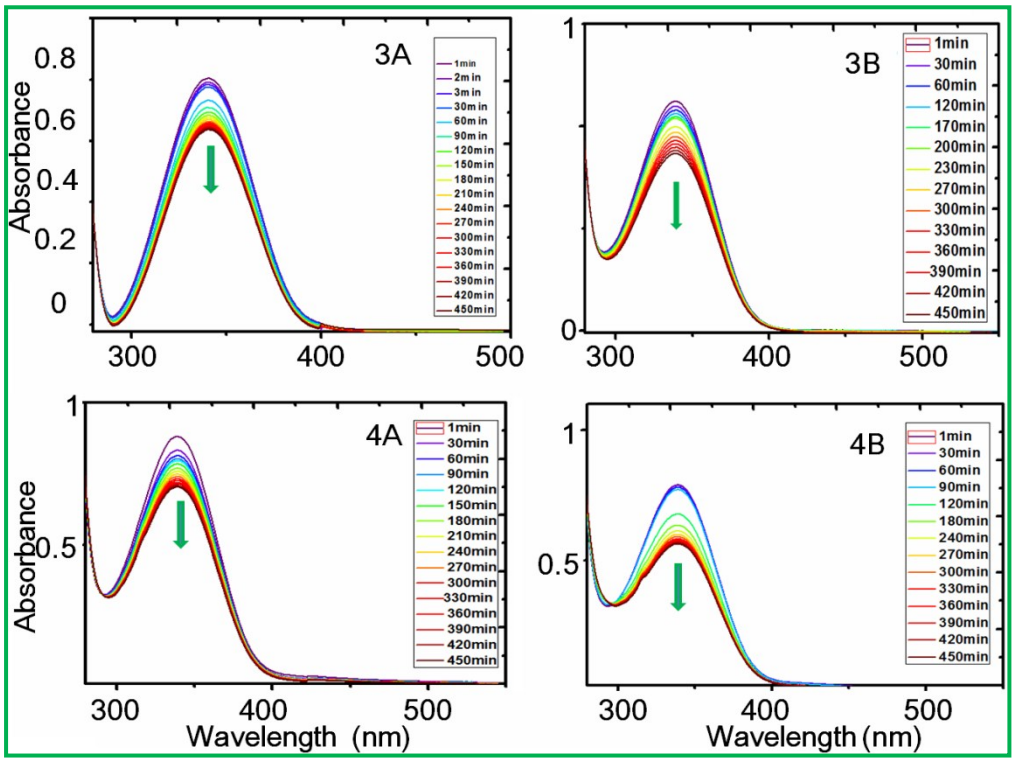

Figure S9. UV-Vis spectra of the reaction of NADH (100 μM) with **3A**, **3B**, **4A** and **4B** (1 μM) in MeOH/H_2O (1:9) at 298 K for 450 min.

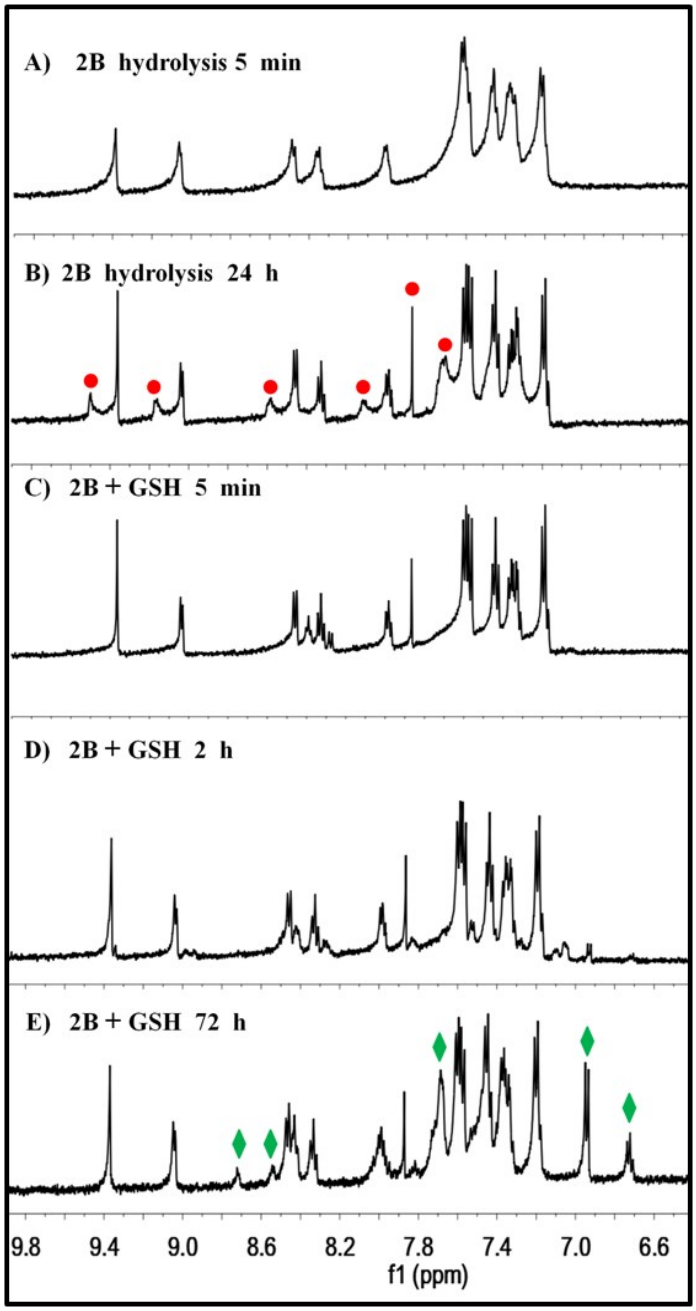

Figure S10. The low field region of ^{1}H NMR spectra for reaction of complex **2B** (2 mM) with GSH (3 mM) in 60% DMSO-d_6/40% D_2O at 310 K. (A) hydrolysis of complex **2B** after 5 min; (B) hydrolysis of complex **2B** after 24 h; (C) reaction of complex **2B** with GSH after 5 min (D) reaction of complex **2B** with GSH after 2 h; (E) reaction of complex **2B** with GSH after 72 h; Peaks labeled ● and ◆ correspond to the new peaks of aqua complex of **2B** after hydrolysis 24 h and the **2B**-GSH adduct respectively.

Table S1. Flow cytometry analysis to determine the percentages of apoptotic cells, using Annexin V -FITC vs PI staining, after exposing A549 cells to complexes **2B** and **4B**.

Complex	Ir concentration	Population (%) Viable	Early apoptosis	Late apoptosis	Non-viable
2B	0.5 × IC_{50}	93.9±0.4	1.5±0.4	4.2±0.4	0.2± 0.1
	1 × IC_{50}	91.3±0.1	3.4±0.1	5.1±0.2	0.2±0.1
	2 × IC_{50}	27.7±0.7	7.6±0.2	63.2±1.3	1.5±0.5
	3 × IC_{50}	3.5±0.2	10.5±0.8	82.1±0.7	3.8±1.5
Control		93.0±0.1	1.2±0.1	5.5±0.3	0.2±0.1

Complex	Ir concentration	Population (%) Viable	Early apoptosis	Late apoptosis	Non-viable
4B	0.5 × IC_{50}	92.0±1.5	3.4±0.8	3.4±0.7	1.1±1.2
	1 × IC_{50}	85.6±0.9	2.8±0.8	8.2±0.3	3.4±0.9
	2 × IC_{50}	68.7±2.1	8.8±0.6	17.2±0.1	5.4±0.8
	3 × IC_{50}	44.1±0.6	13.7±0.2	29.3±1.3	12.9±0.9
Control		95.2±0.9	1.6±1.4	2.1±0.3	1.1±0.6

Table S2. Cell cycle analysis carried out by flow cytometry using PI staining after exposing A549 cells to complexes **2B** and **4B**.

		Population (%)		
Complex	Ir concentration	G_0/G_1 phase	S phase	G_2/M phase
2B	$0.25 \times IC_{50}$	59.3±0.8	27.9±0.5	9.4±0.1
	$0.5 \times IC_{50}$	52.1±0.7	34.1±2.1	10.7±0.8
	$1 \times IC_{50}$	49.6±6.1	37.8±2.5	11.0±1.7
control		61.3±1.3	27.2±1.6	7.5±0.3

		Population (%)		
Complex	Ir concentration	G_0/G_1 phase	S phase	G_2/M phase
4B	$0.25 \times IC_{50}$	52.2±0.1	35.5±1.1	11.0±1.8
	$0.5 \times IC_{50}$	46.8±2.1	37.2±1.5	13.4±1.1
	$1 \times IC_{50}$	46.7±5.8	34.4±5.3	17.3±1.7
control		52.0±0.9	34.1±0.1	11.0±2.2

Table S3. ROS induction in A549 cancer cells treated with complexes **2B** and **4B**.

Complex	Ir concentration	Population (%) Cells in low ROS levels	Cells in high ROS levels
2B	0.25 × IC_{50}	10.8±0.7	89.2±0.7
Untreated cells (**negative control**)		99.3±0.4	0.5±0.4
CCCP treated cells (**positive control**)		17.6±1.3	82.3±1.3

Complex	Ir concentration	Population (%) Cells in low ROS levels	Cells in high ROS levels
4B	0.25 × IC_{50}	8.2±0.5	91.7±0.6
Untreated cells (**negative control**)		99.8±0.2	0.2±0.1
CCCP treated cells (**positive control**)		13.3±1.6	86.2±1.1

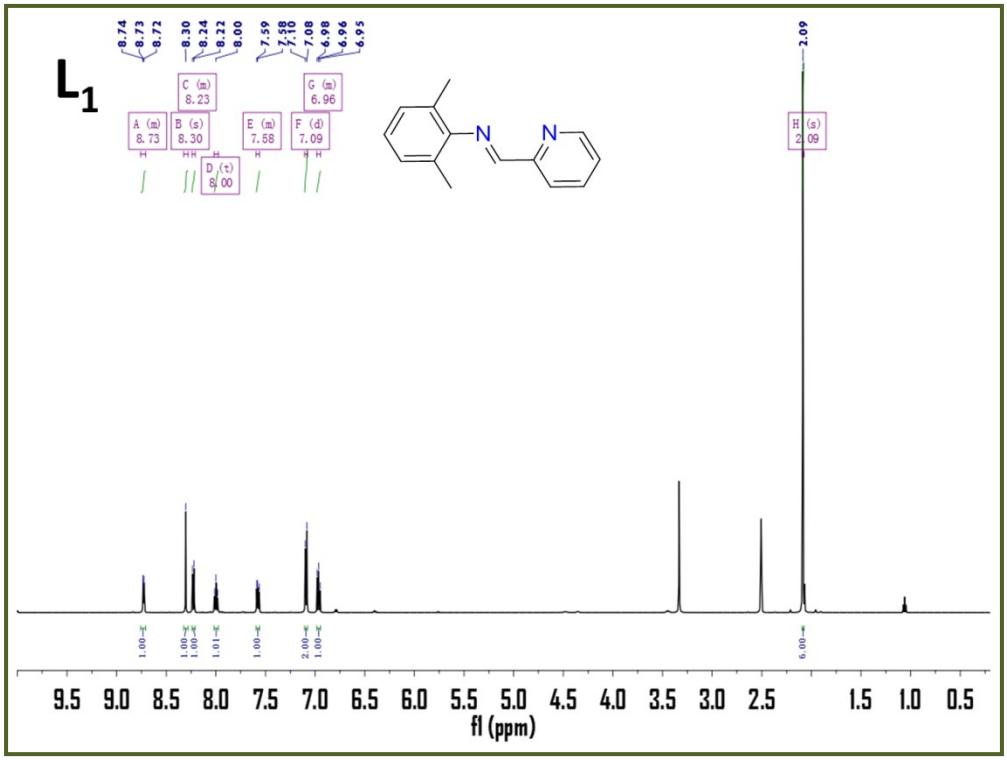

Figure S11. The ^{1}H NMR (500.13 MHz, DMSO) peak integrals of $\mathbf{L_1}$

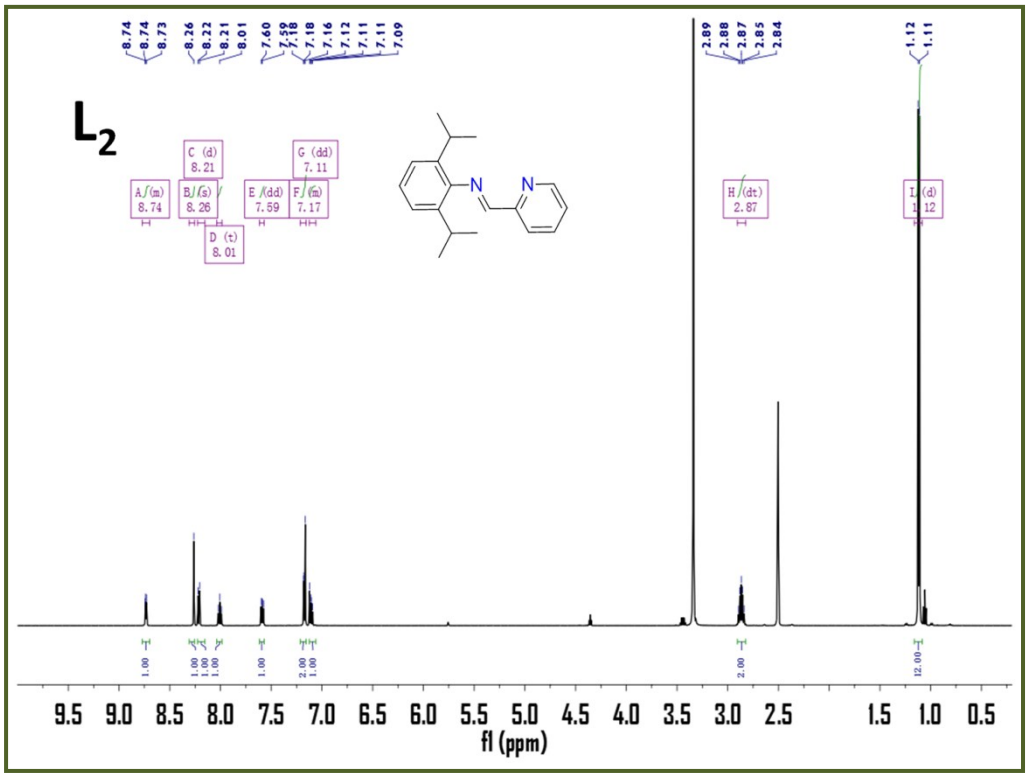

Figure S12. The ^{1}H NMR (500.13 MHz, DMSO) peak integrals of $\mathbf{L_2}$

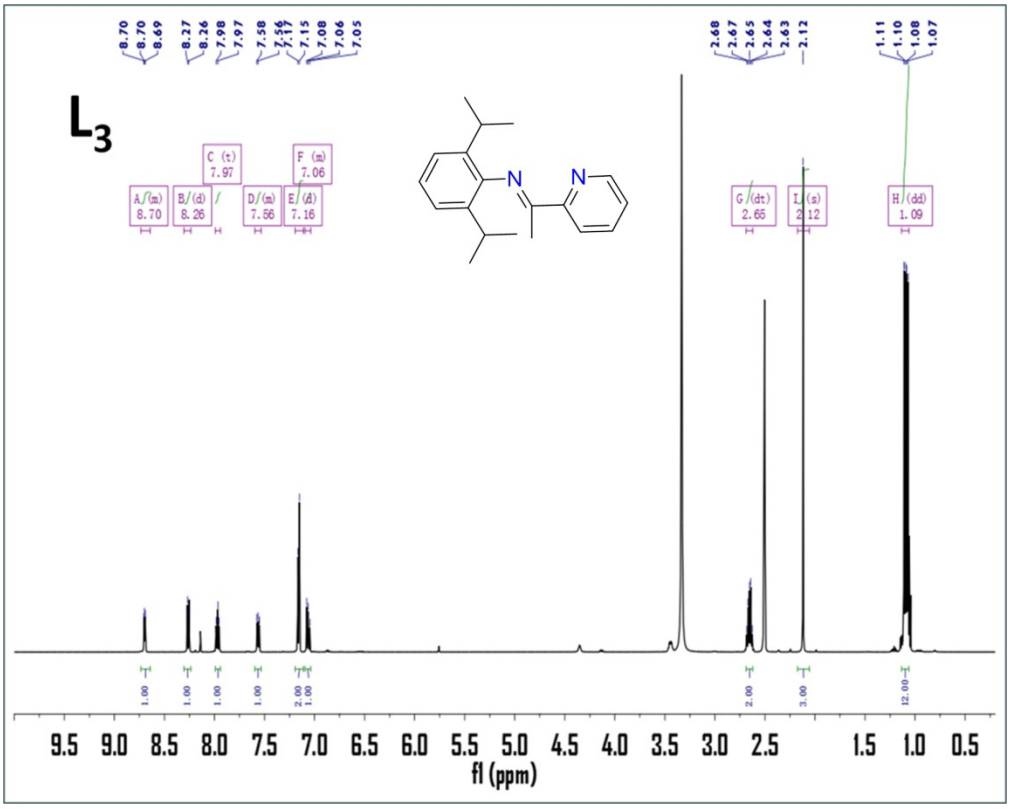

Figure S13. The ^{1}H NMR (500.13 MHz, DMSO) peak integrals of $\mathbf{L_3}$

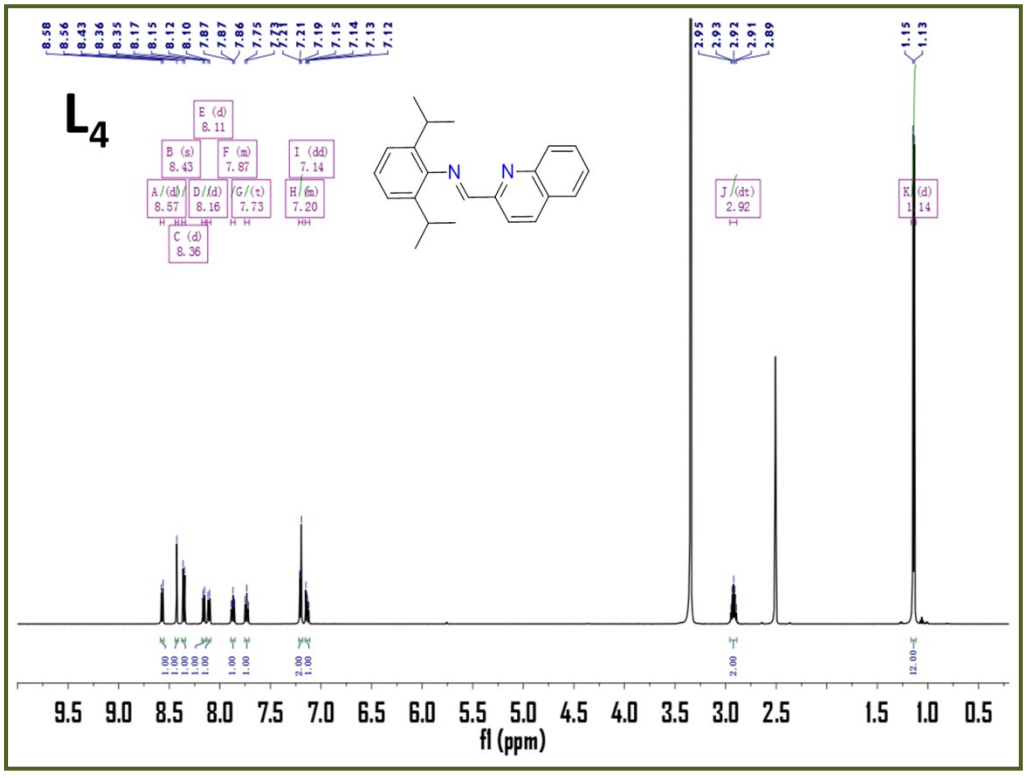

Figure S14. The ^{1}H NMR (500.13 MHz, DMSO) peak integrals of $\mathbf{L_4}$

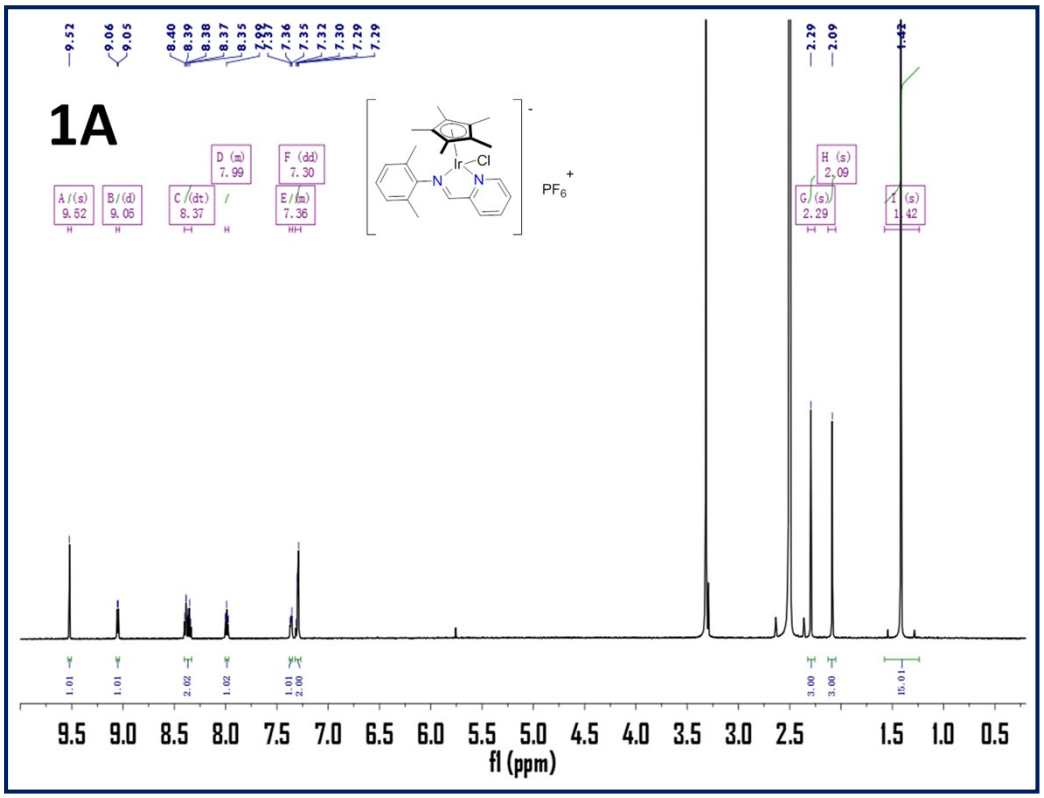

Figure S15. The ^{1}H NMR (500.13 MHz, DMSO) peak integrals of complex **1A** [(η^5-C_5Me_5)Ir(L_1)Cl]PF_6.

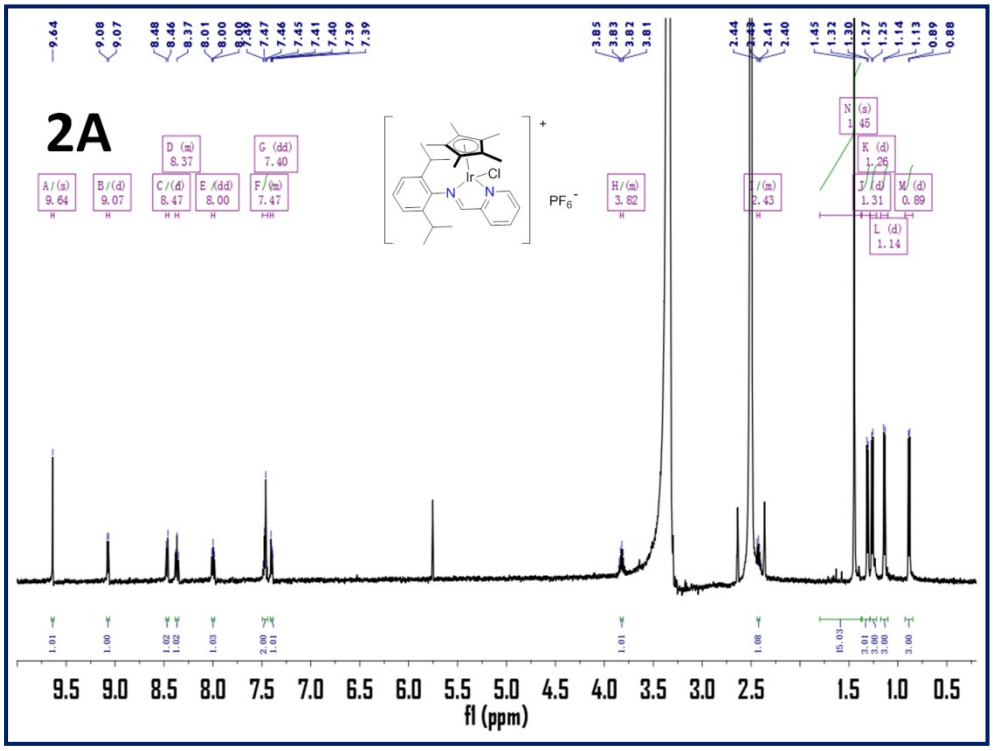

Figure S16. The ^{1}H NMR (500.13 MHz, DMSO) peak integrals of complex **2A** [(η^5-C_5Me_5)Ir(L_2)Cl]PF_6.

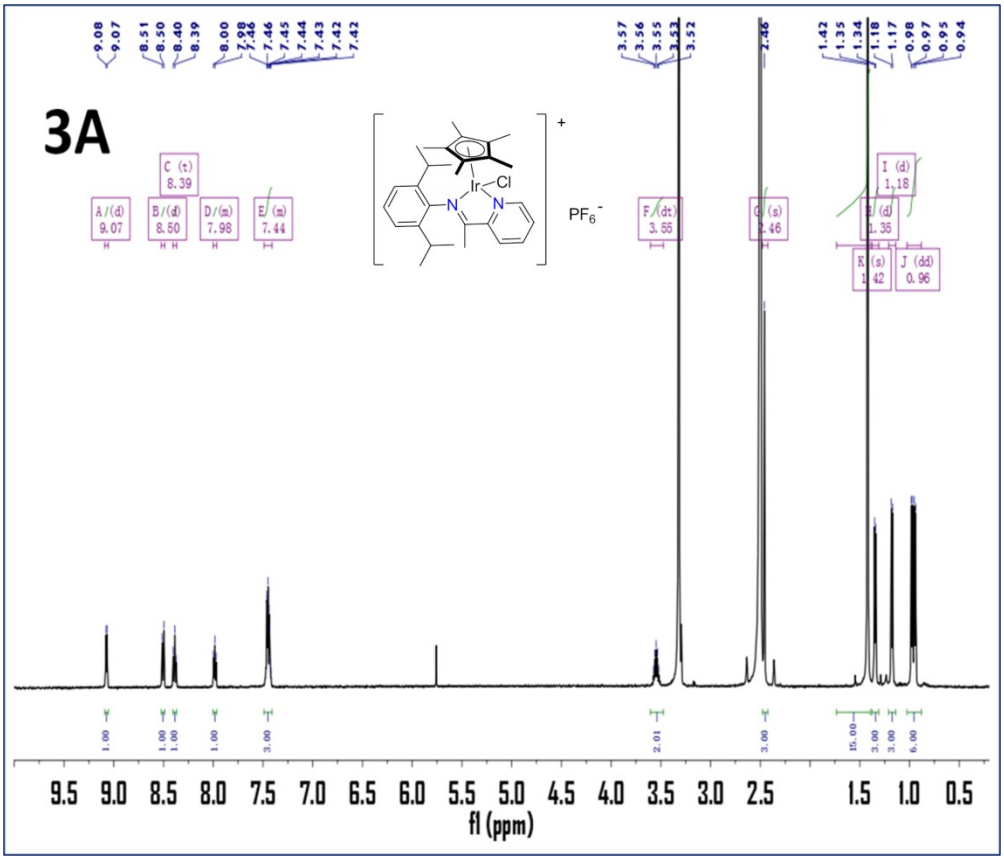

Figure S17. The ^{1}H NMR (500.13 MHz, DMSO) peak integrals of complex **3A** [(η^5-C_5Me_5)Ir(L_3)Cl]PF_6.

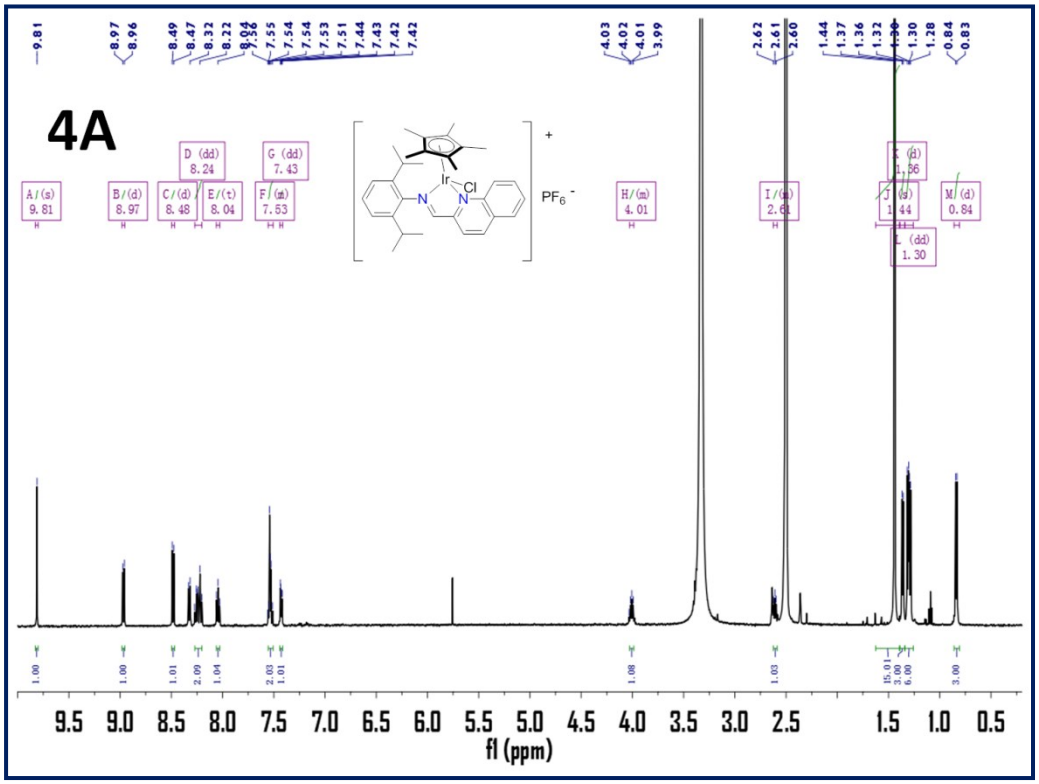

Figure S18. The ^{1}H NMR (500.13 MHz, DMSO) peak integrals of complex **4A** [(η^5-C_5Me_5)Ir(L_4)Cl]PF_6.

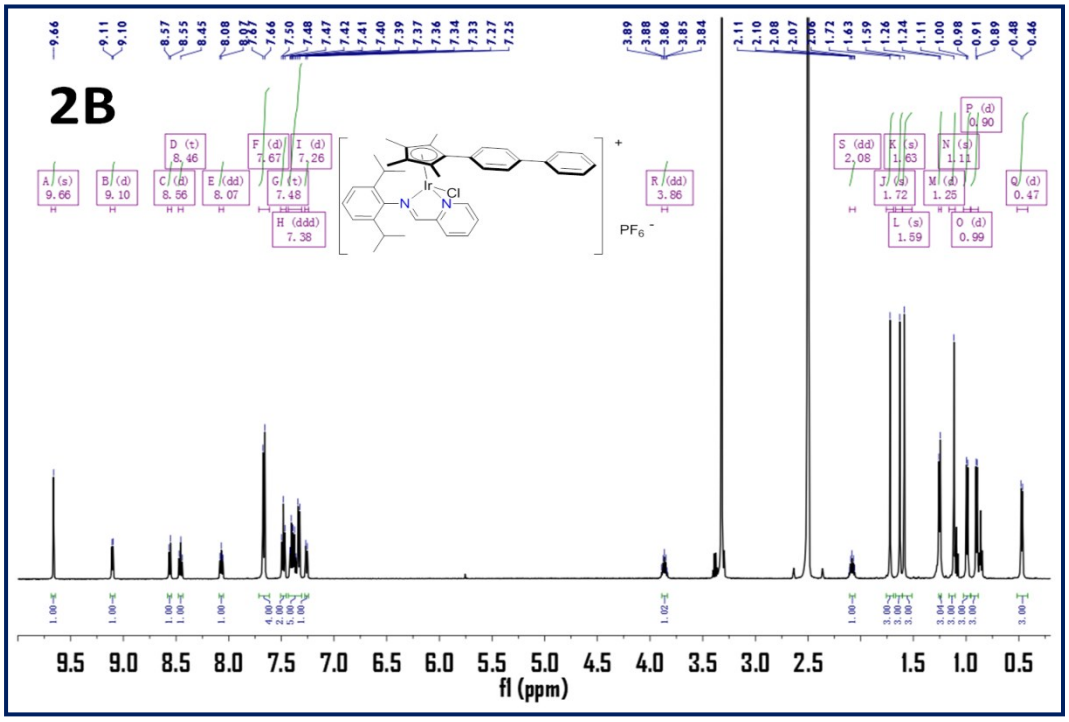

Figure S19. The ^{1}H NMR (500.13 MHz, DMSO) peak integrals at 295 K of complex **2B** [(η^5-$C_5Me_4C_6H_4C_6H_5$)Ir(L_2)Cl]PF_6.

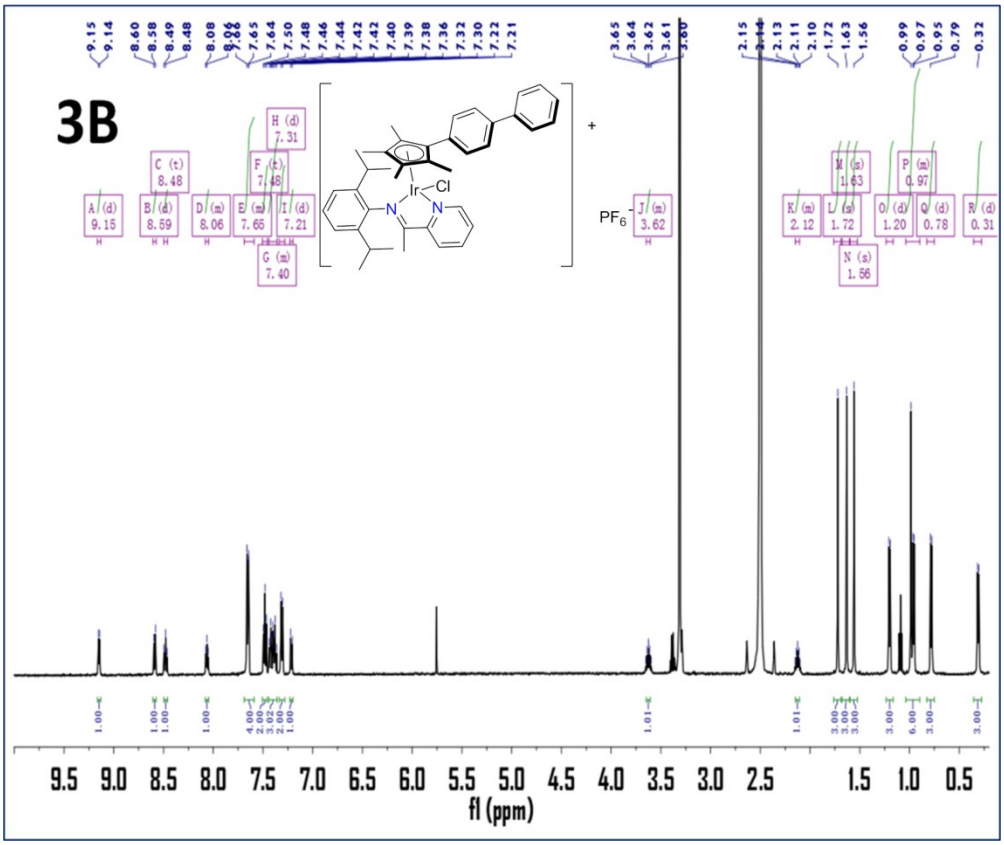

Figure S20. The ^{1}H NMR (500.13 MHz, DMSO) peak integrals at 295 K of complex **3B** [(η^5-$C_5Me_4C_6H_4C_6H_5$)Ir(L_3)Cl]PF_6.

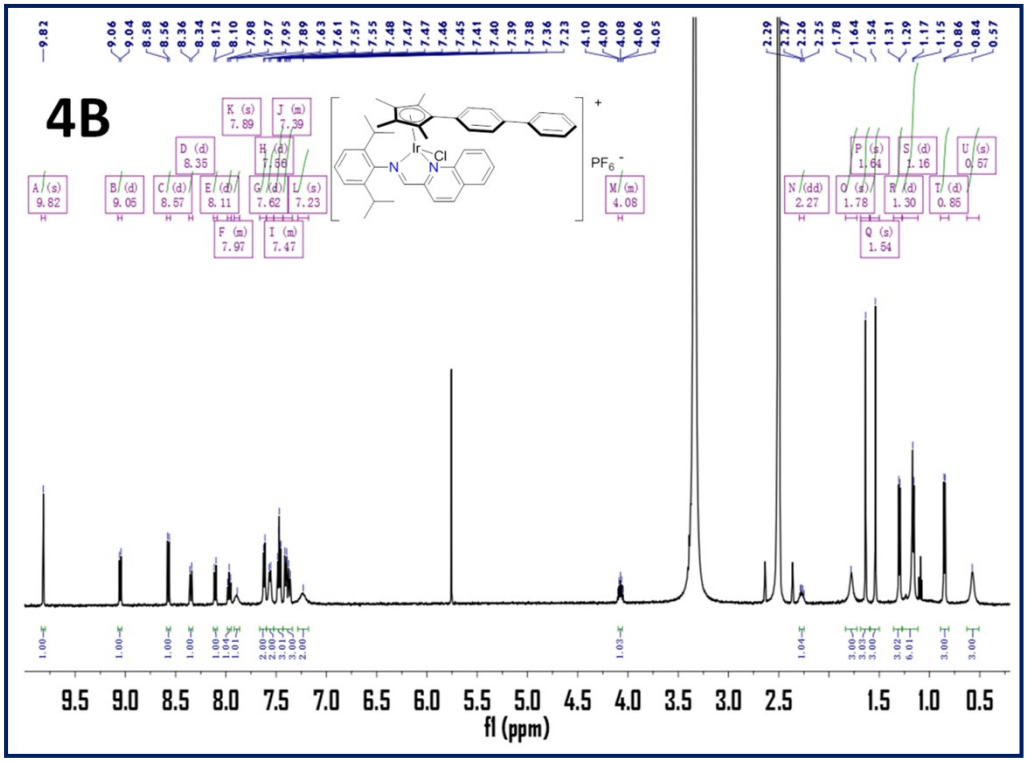

Figure S21. The ^{1}H NMR (500.13 MHz, DMSO) peak integrals at 295 K of complex **4B** [(η^5-$C_5Me_4C_6H_4C_6H_5$)Ir(L_4)Cl]PF_6.

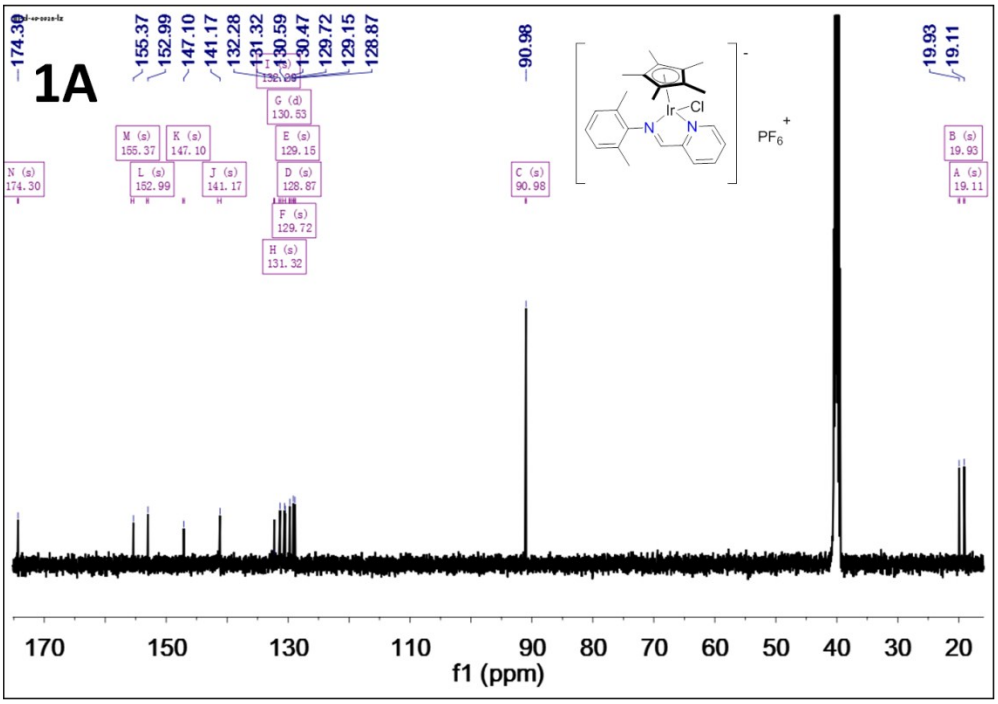

Figure S22. The ^{13}C NMR (126 MHz, DMSO) peak integrals at 295 K of complex **1A** [(η^5-C_5Me_5)Ir(L_1)Cl]PF_6.

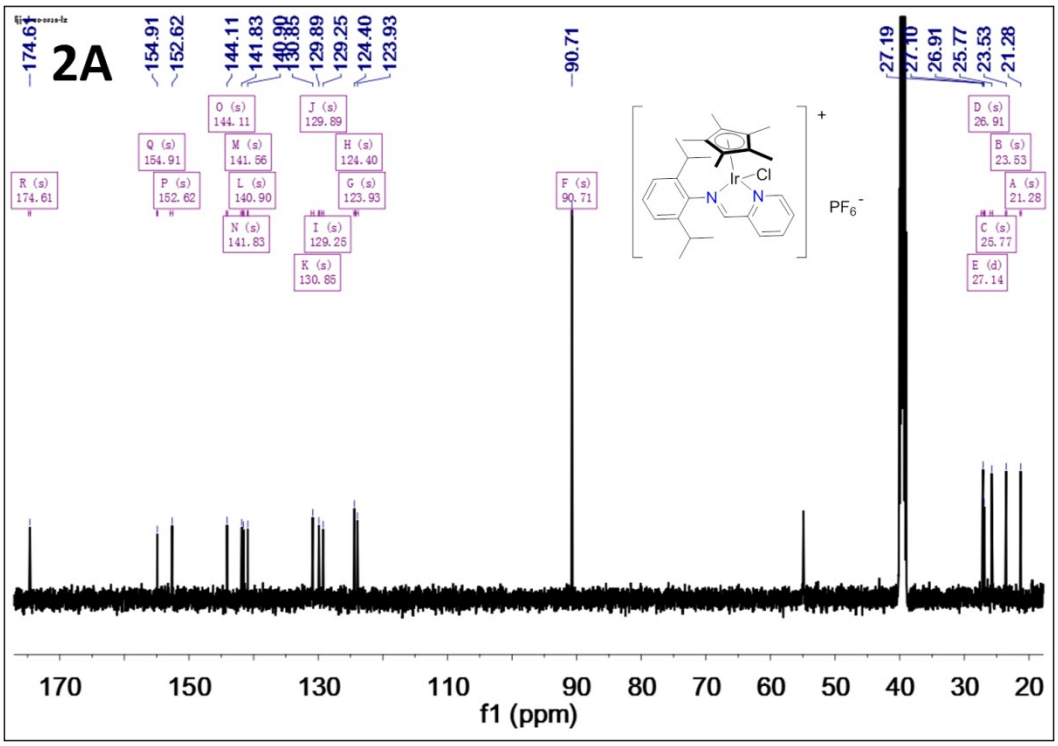

Figure S23. The ^{13}C NMR (126 MHz, DMSO) peak integrals at 295 K of complex **2A** [(η^5-C_5Me_5)Ir(L_2)Cl]PF_6.

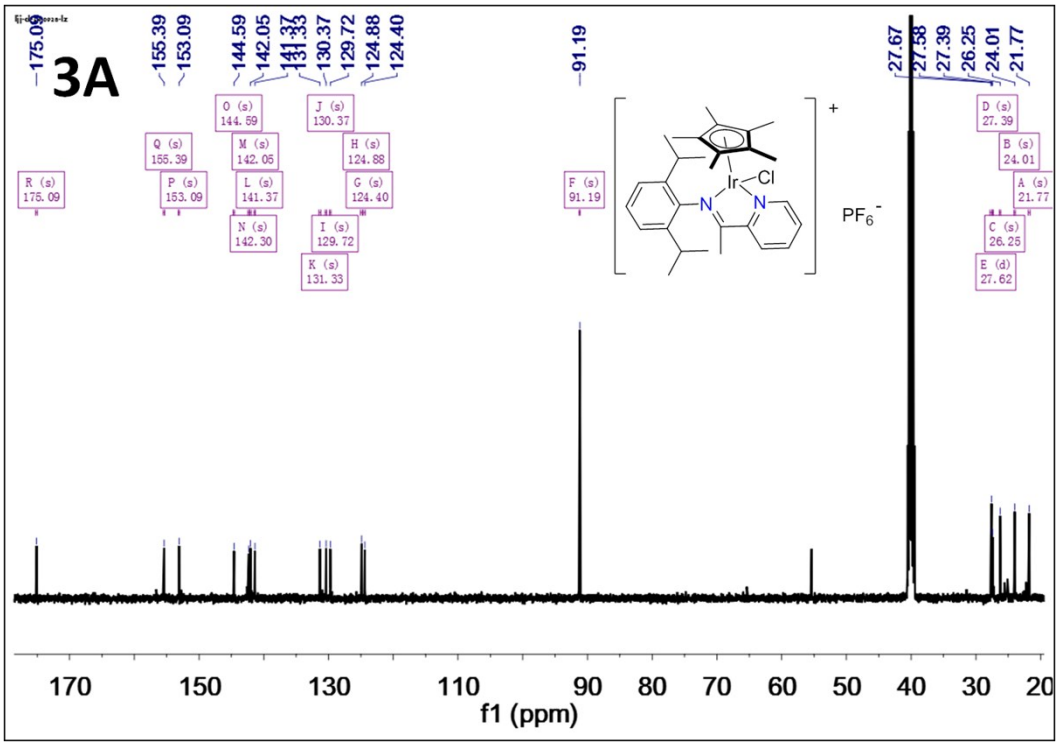

Figure S24. The ^{13}C NMR (126 MHz, DMSO) peak integrals at 295 K of complex **3A** [(η^5-C_5Me_5)Ir(L_3)Cl]PF_6.

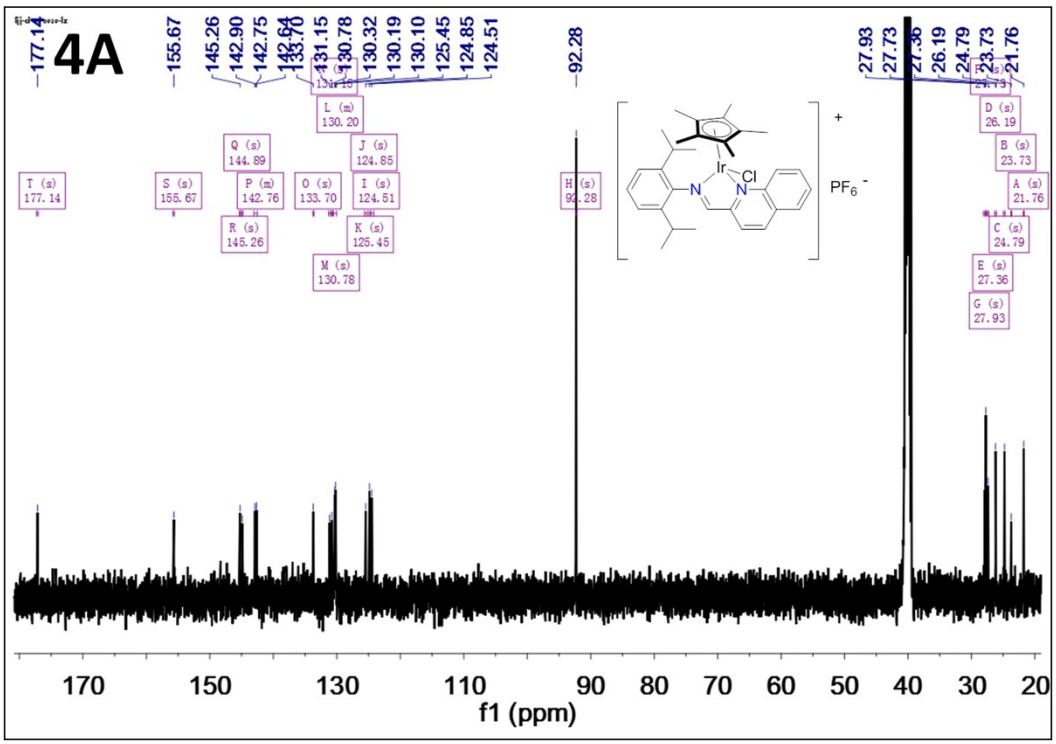

Figure S25. The ^{13}C NMR (126 MHz, DMSO) peak integrals at 295 K of complex **4A** [(η^5-C_5Me_5)Ir(L_4)Cl]PF_6.

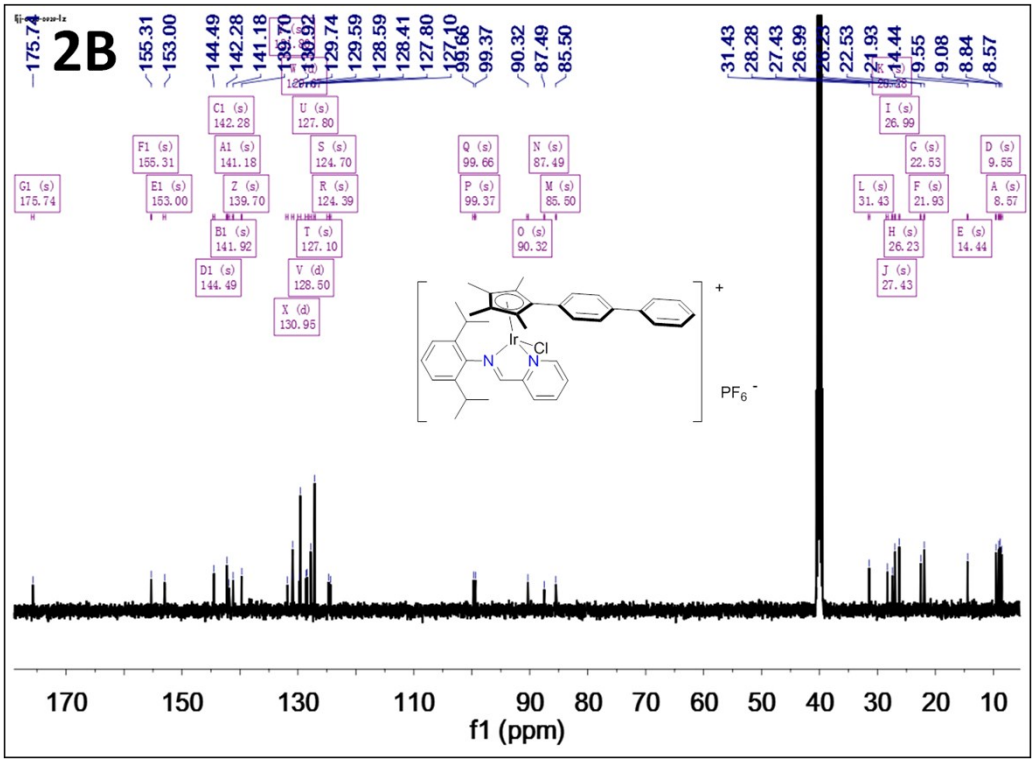

Figure S26. The ^{13}C NMR (126 MHz, DMSO) peak integrals at 295 K of complex **2B** [(η^5-$C_5Me_4C_6H_4C_6H_5$)Ir(L_2)Cl]PF_6.

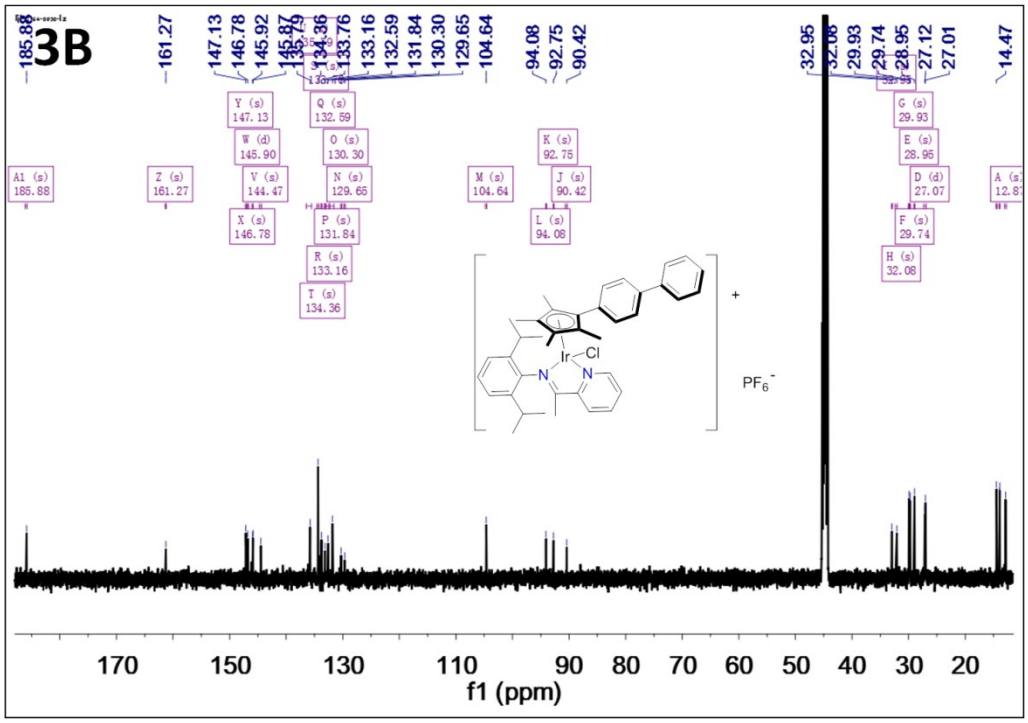

Figure S27. The ^{13}C NMR (126 MHz, DMSO) peak integrals at 295 K of complex **3B** [(η^5-$C_5Me_4C_6H_4C_6H_5$)Ir(L_3)Cl]PF_6.

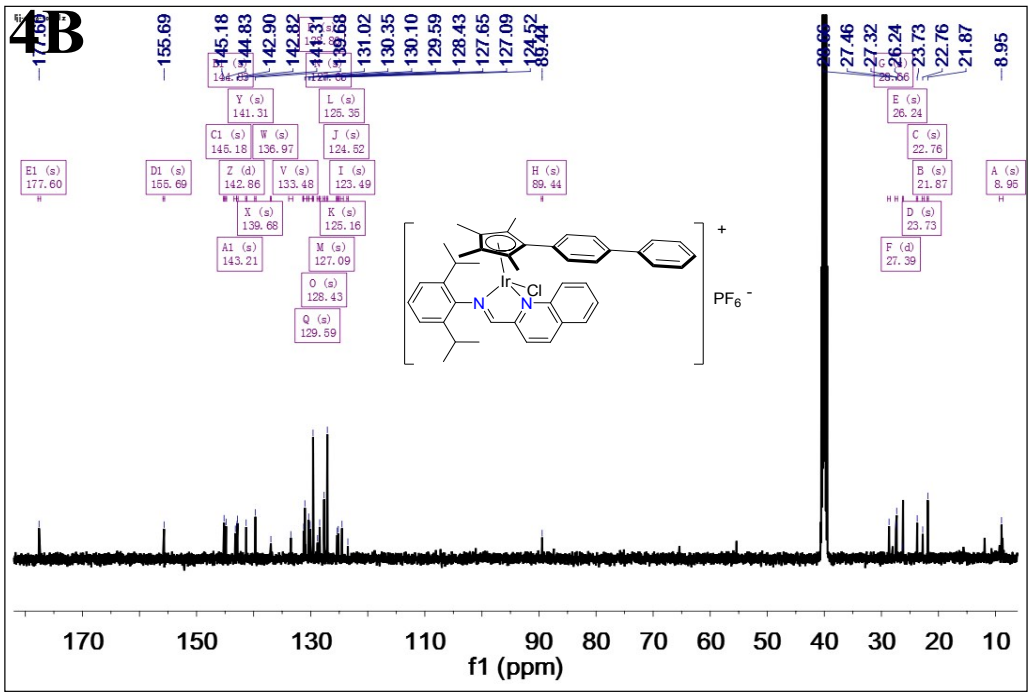

Figure S28. The ^{13}C NMR (126 MHz, DMSO) peak integrals at 295 K of complex **4B** [(η^5-$C_5Me_4C_6H_4C_6H_5$)Ir(L_4)Cl]PF_6.